European Journal of Radiology 118 (2019) 38–43

Contents lists available at ScienceDirect

European Journal of Radiology

journal homepage: www.elsevier.com/locate/ejrad

Research article

# CT texture analysis for the prediction of KRAS mutation status in colorectal cancer via a machine learning approach

Narumi Taguchi[a], Seitaro Oda[a,*], Yasuhiro Yokota[a], Sadahiro Yamamura[b], Masanori Imuta[a], Tadatoshi Tsuchigame[c], Yasunori Nagayama[a], Masafumi Kidoh[a], Takeshi Nakaura[a], Shinya Shiraishi[a], Yoshinori Funama[d], Satoru Shinriki[e], Yuji Miyamoto[f], Hideo Baba[f], Yasuyuki Yamashita[a]

[a] Department of Diagnostic Radiology, Faculty of Life Sciences, Kumamoto University, 1-1-1 Honjyo, Chuo-ku, Kumamoto, 860-8556, Japan
[b] Department of Radiology, Kumamoto General Hospital, 10-10 Tori-cho, Yatsushiro, Kumamoto, 866-8660, Japan
[c] Kumamoto General Health Center, 4-11-1 Higashimachi, Higashi-ku, Kumamoto, 862-0901, Japan
[d] Department of Medical Physics, Faculty of Life Sciences, Kumamoto University, 1-1-1 Honjyo, Chuo-ku, Kumamoto, 860-8556, Japan
[e] Department of Molecular Laboratory Medicine, Faculty of Life Sciences, Kumamoto University, 1-1-1 Honjyo, Chuo-ku, Kumamoto, 860-8556, Japan
[f] Department of Gastroenterological Surgery, Faculty of Life Sciences, Kumamoto University, 1-1-1 Honjyo, Chuo-ku, Kumamoto, 860-8556, Japan

ARTICLE INFO

*Keywords:*
Colorectal cancer
CT texture analysis
Machine learning
KRAS mutation
Radiogenomics

ABSTRACT

*Purpose:* This study aimed to investigate whether a machine learning-based computed tomography (CT) texture analysis could predict the mutation status of V-Ki-ras2 Kirsten rat sarcoma viral oncogene homolog (KRAS) in colorectal cancer.

*Method:* This retrospective study comprised 40 patients with pathologically confirmed colorectal cancer who underwent KRAS mutation testing, contrast-enhancement CT, and $^{18}$F-fluorodeoxyglucose (FDG) positron emission tomography (PET) before treatment. Of the 40 patients, 20 had mutated KRAS genes, whereas 20 had wild-type KRAS genes. Fourteen CT texture parameters were extracted from portal venous phase CT images of primary tumors, and the maximum standard uptake values ($SUV_{max}$) on $^{18}$F-FDG PET images were recorded. Univariate logistic regression was used to develop predictive models for each CT texture parameter and $SUV_{max}$, and a machine learning method (multivariate support vector machine) was used to develop a comprehensive set of CT texture parameters. The area under the receiver operating characteristic (ROC) curve (AUC) of each model was calculated using five-fold cross validation. In addition, the performance of the machine learning method with the CT texture parameters was compared with that of $SUV_{max}$.

*Results:* In the univariate analyses, the AUC of each CT texture parameter ranged from 0.4 to 0.7, while the AUC of the $SUV_{max}$ was 0.58. Comparatively, the multivariate support vector machine with comprehensive CT texture parameters yielded an AUC of 0.82, indicating a superior prediction performance when compared to the $SUV_{max}$.

*Conclusions:* A machine learning-based CT texture analysis was superior to the $SUV_{max}$ for predicting the KRAS mutation status of a colorectal cancer.

## 1. Introduction

Colorectal cancer (CRC) is a major cause of morbidity and mortality worldwide [1]. However, advances in targeted therapy have yielded significant increases in patient survival. Recently, the V-Ki-ras2 Kirsten rat sarcoma viral oncogene homolog (KRAS) mutation status has been identified as an important factor in the treatment of CRC, with several studies reporting that KRAS mutation predicts a lack of response to therapies targeting the epidermal growth factor receptor (EGFR) [2,3]. In recent years, the finding that approximately 40%–45% of CRCs exhibit KRAS mutations [4] has increased interest in the testing of this genetic status.

Currently, the guidelines of the National Comprehensive Cancer Network, European Society for Medical Oncology, and American Society of Clinical Oncology recommend that the tumor tissues of all patients with suspected or proven metastatic CRC should undergo genotyping for KRAS mutations [5–7]. Therefore, identification of the KRAS mutation status of a CRC, either before or during treatment, is

* Corresponding author.
*E-mail address:* seisei0430@nifty.com (S. Oda).

https://doi.org/10.1016/j.ejrad.2019.06.028
Received 11 March 2019; Received in revised form 27 May 2019; Accepted 30 June 2019

required to predict the effects of therapies and determine individual treatment strategies. Although pathologic analyses of the genetic KRAS mutation status are considered the gold standard in current clinical practice, these tests are not always feasible or reliable [8]. Metastatic lesions are often inaccessible and biopsy cores are frequently unsuitable, as poorly cellular specimens are inappropriate for exhaustive molecular examinations. Moreover, primary tumors are often heterogeneous, which may decrease the reliability of KRAS mutation testing.

Previous studies of the relationships between imaging features of CRC and KRAS mutation status have most frequently used positron emission tomography with $^{18}$F-fluorodeoxyglucose ($^{18}$F-FDG PET). However, these studies have yielded conflicting results [9–13]. Recently, radiogenomics using computed tomography (CT) texture analysis, has emerged from the developing research field surrounding the derivation of quantitative imaging features from medical images to predict non-invasively the genetic status, degree of differentiation, and efficacy of chemotherapy in various tumors [14]. Therefore, we hypothesized that the ability to predict the KRAS mutation status of a CRC from CT images would enable precision medicine without subjecting the patient to additional invasive procedures. With this study, we aimed to investigate whether a machine learning-based CT texture analysis could be used to predict the KRAS mutation status of a CRC.

## 2. Materials and methods

### 2.1. Patients

The Institutional Review Board approved the protocol of this retrospective study and waived the requirement for informed consent. The study included 40 patients with pathologically confirmed CRC who underwent KRAS mutation testing, $^{18}$F-FDG PET, and contrast-enhancement CT within 2 months before surgery during the period of March 2013–June 2014. Of the 40 patients, 20 had mutated KRAS genes and 20 had wild-type KRAS genes. Clinical and pathological characteristics, including sex, age, tumor size, degree of tumor differentiation, TNM stage, and C-reactive protein (CRP) level, were recorded (Table 1).

### 2.2. KRAS mutation tests

Genomic DNA was extracted from formalin-fixed paraffin-embedded tumor sections using the cobas DNA Sample Preparation Kit (Roche Molecular Systems, Inc., Branchburg, NJ, USA). KRAS mutations in exons 2, 3, and 4 were detected using a real-time polymerase chain reaction assay, cobas KRAS Mutation Test (Roche Molecular Systems, Inc.), and LightMix KRAS and NRAS kit (Roche Molecular Systems, Inc.). Patients were stratified into two groups according to the test results: mutated KRAS and wild-type KRAS.

**Table 1**
Clinical and pathological analyses.

| | Mutated KRAS group (n = 20) | Wild-type KRAS group (n = 20) | p-value |
|---|---|---|---|
| Sex (male / female) | 11 / 9 | 13 / 7 | 0.53 |
| Age (years) | 67.8 ± 13.4 | 70.8 ± 7.4 | 0.38 |
| Tumor size (cm) | 4.8 ± 1.9 | 4.8 ± 2.5 | 0.97 |
| Tumor differentiation (Well / Moderate / Poor) | 11 / 8 / 1 | 17 / 3 / 0 | 0.03 |
| T (1 / 2 / 3 / 4) | 0 / 0 / 17 / 3 | 0 / 0 / 16 / 4 | 0.76 |
| N (0 / 1 / 2) | 13 / 3 / 4 | 11 / 3 / 6 | 0.47 |
| M (0 / 1) | 13 / 7 | 14 / 6 | 0.74 |
| Stage (I / II / III / IV) | 0 / 10 / 3 / 7 | 0 / 10 / 4 / 6 | 0.74 |
| CRP (mg/dl) | 0.50 ± 0.68 | 1.30 ± 2.19 | 0.13 |

*Note:* Data are shown as means ± standard deviations. KRAS: V-Ki-ras2 Kirsten rat sarcoma viral oncogene homolog, CRP: C-reactive protein.

### 2.3. $^{18}$F-FDG PET examinations

All patients underwent whole-body $^{18}$F-FDG PET scanner (Gemini-GXL 16, Philips Healthcare, MA, USA) after fasting for at least 5 h before tracer administration. Sixty minutes prior to the scan, each patient received an intravenous injection of approximately 186–256 MBq of $^{18}$F-FDG. During the subsequent whole-body emission scan, each region (one bed position: 18 cm) was scanned for 1.5 min. As each bed position overlapped the next position by 50%, imaging data were acquired for 3 min at almost all the bed positions. A 144 × 144 matrix and LOR-RAMLA reconstruction parameters were used, with a reconstruction section thickness and section interval of 5.0 mm. A circular region of interest (ROI) was placed manually on the CRC, and the maximum standardized uptake value ($SUV_{max}$) was calculated for each lesion.

### 2.4. CT scanning and image reconstruction

All patients were examined using one of two multi-detector row CT systems (Brilliance-64, Philips Healthcare or Aquilion ONE ViSION, Canon Medical Systems, Otawara, Japan) after the delivery of a standard contrast material dose (600 mgI/kg) over 35 s. Scanning was initiated at 40 (early phase) and 80 s (portal venous phase) after contrast material injection. For all examinations, iohexol (Omnipaque 300; Daiichi-Sankyo, Tokyo, Japan) or iopamidol (Iopamiron 300 or 370; Bayer Healthcare, Osaka, Japan) was delivered via a 22-G catheter inserted into an antecubital vein and a power injector (Dual Shot GX V; Nemoto Kyorindo, Tokyo, Japan). The scan parameters for the Brilliance-64 scanner were as follows: detector configuration, 64 × 0.625 mm (detector collimation); gantry rotation time, 0.5 s; helical pitch (beam pitch), 0.769; and tube voltage, 120 kVp. The tube potential and tube current were determined using automatic exposure control (Dose Right; Philips Healthcare) and based on X-ray attenuation on anteroposterior and lateral scout images, with a reference tube current time product of 285 mAs (effective). The parameters for the Aquilion ONE ViSION scanner were as follows: detector configuration, 80 × 0.5 mm; gantry rotation time, 0.5 s; helical pitch, 0.813; and tube voltage, 120 kVp. An automatic tube current modulation program (SURE Exposure 3D, Canon Medical Systems) was used, and the noise index (one standard deviation [SD] of the regional CT radiodensity value) was set at 10 Hounsfield units for images with a slice thickness of 5.0 mm.

Images were reconstructed in a 30–35 cm field-of-view display (dependent on the patient's physique). Both the reconstruction section thickness and section interval were 5.0 mm. CT images from both scanners were reconstructed using the following hybrid-type iterative reconstruction algorithms: iDose$^4$ (Philips Healthcare) in "level 3″ mode with kernel C for the Brilliance-64 scanner and AIDR-3D (Canon Medical Systems) in "weak" mode with kernel FC03 for the Aquilion ONE ViSION scanner.

### 2.5. CT texture measurements

To compute the texture parameters, DICOM image files of 40 tumors were imported to the software package LIFEx (version 2.00, http://www.lifexsoft.org/). Next, the outer edge of each tumor was manually traced on the axial slice from portal venous phase CT that yielded the maximum tumor area, and this ROI was selected for the CT texture analysis (Fig. 1). LIFEx was used to extract 14 CT texture parameters from the primary tumors.

### 2.6. Statistical analysis

Numerical data are expressed as means ± SDs. Between-group differences in the mean values of normally and non-normally distributed data were determined using the two-tailed independent *t*-test and the Mann–Whitney U-test, respectively. The $\chi^2$ test was also used

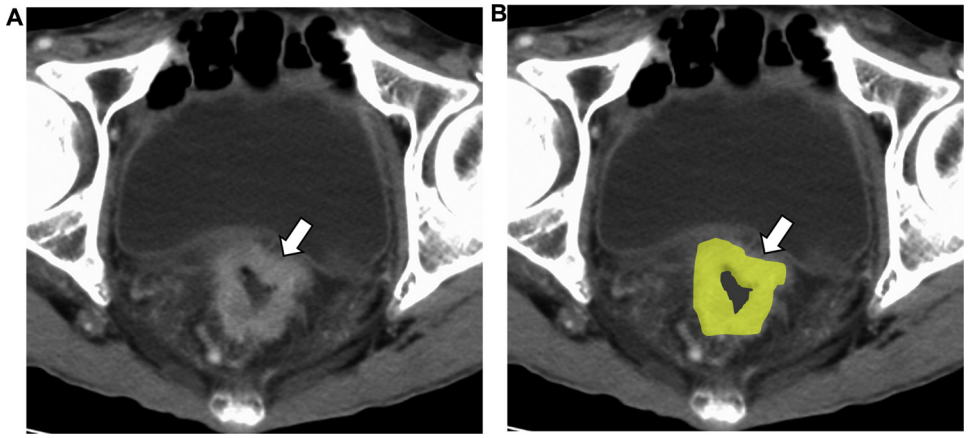


**Fig. 1.** Measurements of texture on computed tomography (CT) images from a patient with rectal cancer. (a) A portal venous phase CT image reveals an irregular mass in the rectum. (b) A region of interest was drawn manually along the outer edge of the tumor.

for between-group comparisons. Univariate logistic regression was used to develop KRAS mutation status prediction models for each CT texture parameter and $SUV_{max}$. Next, a machine learning method-based (multivariate support vector machine) prediction model of the comprehensive CT texture parameters was developed. The area under the receiver operating characteristic (ROC) curve (AUC) of each prediction model was calculated using five-fold cross validation, and the predictive performance of the machine learning method with comprehensive CT texture parameters was compared to that of the $SUV_{max}$. The probability of detection of KRAS mutation was also calculated using the machine learning method with comprehensive CT texture parameters and univariate logistic regression for the $SUV_{max}$. A P-value of $< 0.05$ was considered statistically significant. Statistical analyses were performed using Python programing software (version 3.5; https://www.python.org/) and a statistics software package for Microsoft Excel (BellCurve for Excel; SSRI, Tokyo, Japan).

## 3. Results

### 3.1. Clinical and pathological analysis

The patients' characteristics are summarized in Table 1. There were no demographic differences between the mutated and wild-type *KRAS* groups in terms of sex, age, tumor size, TNM stage, or CRP level. However, the two groups differed with respect to tumor differentiation.

### 3.2. Predictive model analysis

In the univariate analyses, the AUCs of each CT texture parameter ranged from 0.40 to 0.71, while the $SUV_{max}$ yielded an AUC of 0.58 (Table 2). Skewness (H) and max value were statistically significantly associated with the KRAS mutation status. Comparatively, the multivariate support vector machine with comprehensive CT texture parameters yielded an AUC of 0.82, indicating a superior prediction performance (Fig. 2). Representative cases of mutated KRAS and wild-type KRAS CRC are shown in Fig. 3 and 4.

## 4. Discussion

Our results demonstrate that each CT texture parameter and the $SUV_{max}$ yielded relatively low AUC values (0.40–0.71) for prediction of KRAS mutation status, however our multivariate machine learning method, which included 14 CT texture parameters, yielded a significantly higher AUC (0.82) and thus a superior prediction performance when compared to the $SUV_{max}$.

Approximately 20% patients with CRC initially present with metastatic disease, and up to 50% of early-stage tumors will eventually metastasize [15]. Although chemotherapy is the main treatment for both metastatic and local advanced-stage CRC, patients with a poor prognosis may be unable to tolerate the associated toxicity and adverse side effects. In comparison, anti-EGFR monoclonal antibody therapy is associated with improvements in both prognosis and compliance, as well as reductions in toxicity and side effects [16]. For example, Heinemann et al. reported that patients with KRAS wild-type metastatic CRC who received anti-EGFR monoclonal antibody therapy (cetuximab) and the FOLFIRI regimen (folinic acid, 5-fluorouracil, irinotecan) experienced a prolongation of survival to 33.1 months [17]. However, anti-EGFR monoclonal antibodies are relatively expensive. Major clinical practice guidelines have explicitly identified KRAS mutation as a highly specific negative biomarker indicating patients who would benefit from anti-EGFR monoclonal antibody therapy [5]. Therefore, the identification of these patients prior to treatment is a critical means of ensuring the delivery of precise and cost-effective medicine to patients with CRC.

Although anti-EGFR monoclonal antibodies have been administered for KRAS wild-type CRC, up to 50% of these patients are unresponsive to this therapy [2]. This treatment failure may be attributable to intratumoral KRAS mutation heterogeneity [18]; in other words, pathologic KRAS mutation tests may not reflect the macroscopic status of the whole tumor. Moreover, metastatic lesions are often inaccessible and biopsy cores are frequently unsuitable [18]. By contrast, CT can be used to image the whole tumor and may be useful as a supplement to genotypic analyses. Our results indicate that CT texture parameters may help to predict the KRAS mutation statuses of patients with CRC and could facilitate the determination of therapeutic strategies.

Previous studies have used $^{18}$F-FDG PET to assess the associations with KRAS mutation status in CRC [9–13]. Several studies concluded that $^{18}$F-FDG PET may be useful for predicting the KRAS mutation status. Iwamoto et al. suggested that upregulated glucose transporter-1 expression might explain the increased $^{18}$F-FDG accumulation in KRAS-mutated CRCs [19]. By contrast, however, several studies of CRC found no significant correlation of $^{18}$F-FDG accumulation with the KRAS mutation status. The reasons for this discrepancy are unknown, although the effects of sample size and ethnic differences cannot be ruled out. Lee et al. suggested that among patients with normal CRP levels, KRAS mutation was associated with a higher $SUV_{max}$, compared to wild-type KRAS, whereas the reverse was true among patients with elevated CRP levels [20]. In other words, local inflammation may affect $^{18}$F-FDG uptake by a CRC, and elevated CRP levels may indicate false-positive $^{18}$F-FDG PET findings. In our study, we observed no differences in the CRP level between the mutated and wild-type KRAS groups. More recently, Kim et al. conducted a systematic review and meta-analysis of

**Table 2**
Univariate logistic regression analysis of CT texture parameters and $SUV_{max}$.

| | | Mutated KRAS group (n = 20) | Wild-type KRAS group (n = 20) | p-value | AUC |
|---|---|---|---|---|---|
| CT texture parameters | Minimum value | −10.2 ± 21.7 | 1.9 ± 20.4 | 0.07 | 0.63 |
| | Mean value | 71.5 ± 12.2 | 78.0 ± 12.4 | 0.10 | 0.62 |
| | Standard deviation | 18.0 ± 3.5 | 18.4 ± 4.0 | 0.71 | 0.40 |
| | Max value | 119.4 ± 18.6 | 131.4 ± 17.7 | 0.04 | 0.68 |
| | Skewness (H) | −0.65 ± 0.34 | −0.39 ± 0.30 | 0.01 | 0.71 |
| | Kurtosis (H) | 4.18 ± 1.70 | 3.54 ± 0.66 | 0.13 | 0.57 |
| | Entropy (H) | 1.83 ± 0.09 | 1.82 ± 0.09 | 0.88 | 0.42 |
| | Energy (H) | 0.017 ± 0.004 | 0.018 ± 0.004 | 0.88 | 0.45 |
| | Homogeneity | 0.61 ± 0.04 | 0.59 ± 0.04 | 0.16 | 0.58 |
| | Energy | 0.044 ± 0.02 | 0.039 ± 0.01 | 0.34 | 0.52 |
| | Contrast | 2.01 ± 0.65 | 2.32 ± 0.77 | 0.18 | 0.57 |
| | Correlation | 0.67 ± 0.09 | 0.63 ± 0.12 | 0.19 | 0.62 |
| | Entropy | 1.53 ± 0.15 | 1.56 ± 0.12 | 0.51 | 0.47 |
| | Dissimilarity | 1.04 ± 0.19 | 1.12 ± 0.19 | 0.17 | 0.59 |
| $^{18}$F-FDG PET parameter | $SUV_{max}$ | 14.2 ± 7.46 | 15.9 ± 5.18 | 0.39 | 0.58 |

*Note:* Data are shown as means ± standard deviations. (H): histogram features, KRAS: V-Ki-ras2 Kirsten rat sarcoma viral oncogene homolog, AUC: area under the receiver operating characteristic curve, CT: computed tomography, $^{18}$F-FDG PET: positron emission tomography with $^{18}$F-fluorodeoxyglucose, $SUV_{max}$: maximum standardized uptake value.

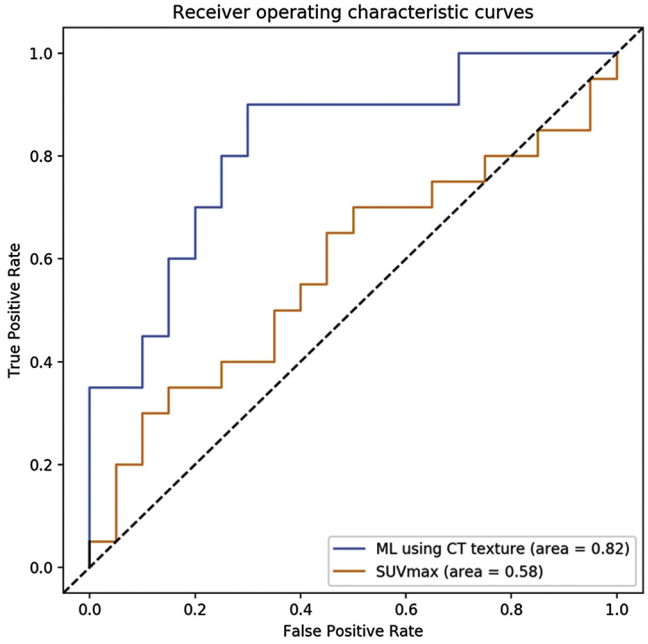


**Fig. 2.** Receiver operating characteristic (ROC) curve analysis comparing the predictions of KRAS mutation status in CRC based on the machine learning-based approach with comprehensive computed tomography (CT) texture parameters and the maximum standard uptake value ($SUV_{max}$). The respective ROC curves are shown in blue and orange. The machine learning method yielded an area under the curve (AUC) of 0.82, which indicating a superior prediction performance when compared to the $SUV_{max}$ (AUC = 0.58).

the ability of $^{18}$F-FDG PET to predict KRAS mutation in CRC and reported that this technique was poorly sensitive and specific [21]. The authors concluded that $^{18}$F-FDG PET might not be useful for predicting or excluding the KRAS mutation status. Therefore, the use of $^{18}$F-FDG PET to predict the KRAS mutation status in CRC patients should be applied and interpreted cautiously.

Previous studies have also investigated the relationship between magnetic resonance imaging (MRI) characteristics and the KRAS mutation status of CRC [22–25]. Meng et al. reported an association of radiomics features extracted from multiparametric MRI with the KRAS mutation status [22]. Xu et al. evaluated the relative diagnostic potential of diffusion-weighted MRI parameters for predicting KRAS mutation status in CRC patients. Notably, these MRI-derived parameters exhibited a moderately significant ability to predict the KRAS mutation status. Further developments in this area are expected in the future.

In a recent investigation, Yang et al. reported an association between the CT texture signatures and the predicted KRAS mutation status of CRC when using a machine learning approach [26]. In that study, the support vector machine model yielded accuracies of 0.787 (95% CI, 0.669–0.871; sensitivity, 0.757; specificity, 0.833) and 0.750 (95% CI, 0.623–0.845; sensitivity, 0.686; specificity, 0.857) for differentiating the mutated group from the wild-type group in the primary and validation cohorts, respectively. Our results were consistent with those findings, and to the best of our knowledge, our report was the first to determine the superiority of the CT texture signature over the $^{18}$F-FDG PET $SUV_{max}$ for predicting the KRAS mutation status of CRC.

We note that our single-center retrospective study had some limitations. First, our sample size was small, and we could not prepare separate training and validation cohorts. Therefore, we calculated the diagnostic performance in a single cohort using five-fold cross validation. However, the accuracy of the prediction models and generalization performance may be inadequate due to the small sample size. Large-scale clinical studies with training and validation cohorts are needed to increase the robustness of our findings. Second, we only evaluated ability to predict the KRAS mutation status and did not investigate mutations in other genes (e.g., NRAS, BRAF). However, previous studies have shown up to 65% of CRCs with wild-type KRAS fail to respond to anti-EGFR monoclonal antibodies, suggesting the involvement of mutations in other regions of the gene or in other genes encoding proteins that act downstream of EGFR in the RAS signaling pathway [27]. Therefore, CRCs harboring wild-type KRAS should also be subjected to NRAS and BRAF mutation analyses [7], and the applicability of CT texture analysis for the predictions of these mutations should be explored. Third, we used a 2D texture analysis, rather than a 3D analysis. Although one previous study reported similar CT texture results following 2D and 3D analyses [28], another study found that a 3D analysis may provide a more representative evaluation of tumor heterogeneity [29]. Hence, further studies are necessary to confirm our findings. Finally, we used only one software package for the CT texture analysis and one machine learning method. Therefore, the applicability of our findings to other software and machine learning methods is uncertain.

## 5. Conclusions

In conclusion, we found that a machine learning approach based on comprehensive CT texture features exhibited a superior performance for the prediction of the KRAS mutation status in CRC when compared to the $^{18}$F-FDG-PET $SUV_{max}$.

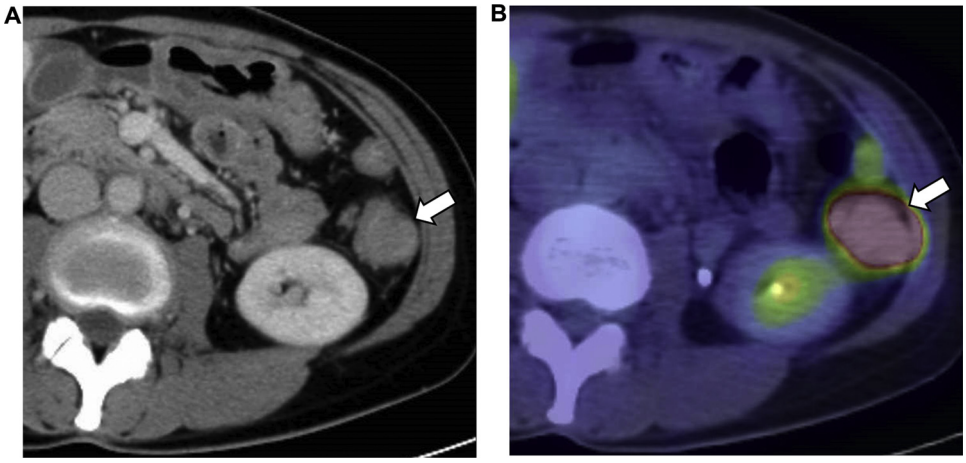


**Fig. 3.** A 41-year-old woman with KRAS-mutated sigmoid colon cancer. Axial computed tomography (CT) image in the portal venous phase (a). $^{18}$F-fluorodeoxyglucose positron emission tomography/CT fusion image (b). The lesion had a maximum standard uptake value ($SUV_{max}$) of 14.7, and the comprehensive CT texture parameters and $SUV_{max}$ yielded probabilities of KRAS mutation of 0.83 and 0.48, respectively.

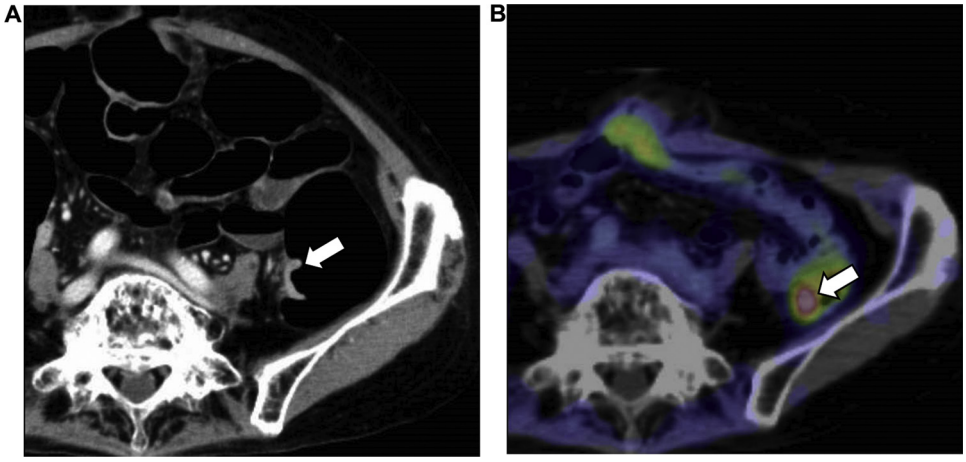


**Fig. 4.** A 72-year-old man with a KRAS wild-type sigmoid colon cancer. Axial computed tomography (CT) image in the portal venous phase (a). $^{18}$F-fluorodeoxyglucose positron emission tomography/CT fusion image (b). The lesion had a maximum standard uptake value ($SUV_{max}$) of 7.1, and the comprehensive CT texture parameters and $SUV_{max}$ yielded probabilities of KRAS mutation of 0.29 and 0.57, respectively.

## References


[1] T. Shinagawa, T. Tanaka, H. Nozawa, S. Emoto, K. Murono, M. Kaneko, K. Sasaki, K. Otani, T. Nishikawa, K. Hata, K. Kawai, T. Watanabe, Comparison of the guidelines for colorectal cancer in Japan, the USA and Europe, Ann. Gastroenterol. Surg. 2 (1) (2018) 6–12.

[2] A. Lievre, J.B. Bachet, V. Boige, A. Cayre, D. Le Corre, E. Buc, M. Ychou, O. Bouche, B. Landi, C. Louvet, T. Andre, F. Bibeau, M.D. Diebold, P. Rougier, M. Ducreux, G. Tomasic, J.F. Emile, F. Penault-Llorca, P. Laurent-Puig, KRAS mutations as an independent prognostic factor in patients with advanced colorectal cancer treated with cetuximab, J. Clin. Oncol. 26 (3) (2008) 374–379.

[3] C.S. Karapetis, S. Khambata-Ford, D.J. Jonker, C.J. O'Callaghan, D. Tu, N.C. Tebbutt, R.J. Simes, H. Chalchal, J.D. Shapiro, S. Robitaille, T.J. Price, L. Shepherd, H.J. Au, C. Langer, M.J. Moore, J.R. Zalcberg, K-ras mutations and benefit from cetuximab in advanced colorectal cancer, N. Engl. J. Med. 359 (17) (2008) 1757–1765.

[4] M. Peeters, G. Kafatos, A. Taylor, V.M. Gastanaga, K.S. Oliner, G. Hechmati, J.H. Terwey, J.H. van Krieken, Prevalence of RAS mutations and individual variation patterns among patients with metastatic colorectal cancer: A pooled analysis of randomised controlled trials, Eur. J. Cancer 51 (13) (2015) 1704–1713.

[5] A.B. Benson 3rd, A.P. Venook, M.M. Al-Hawary, L. Cederquist, Y.J. Chen, K.K. Ciombor, S. Cohen, H.S. Cooper, D. Deming, P.F. Engstrom, I. Garrido-Laguna, J.L. Grem, A. Grothey, H.S. Hochster, S. Hoffe, S. Hunt, A. Kamel, N. Kirilcuk, S. Krishnamurthi, W.A. Messersmith, J. Meyerhardt, E.D. Miller, M.F. Mulcahy, J.D. Murphy, S. Nurkin, L. Saltz, S. Sharma, D. Shibata, J.M. Skibber, C.T. Sofocleous, E.M. Stoffel, E. Stotsky-Himelfarb, C.G. Willett, E. Wuthrick, K.M. Gregory, D.A. Freedman-Cass, NCCN guidelines insights: colon Cancer, version 2.2018, J. Compr. Canc. Netw. 16 (4) (2018) 359–369.

[6] E. Van Cutsem, A. Cervantes, B. Nordlinger, D. Arnold, Metastatic colorectal cancer: ESMO Clinical Practice Guidelines for diagnosis, treatment and follow-up, Ann. Oncol. 25 (Suppl 3) (2014) iii1–iii9.

[7] C.J. Allegra, J.M. Jessup, M.R. Somerfield, S.R. Hamilton, E.H. Hammond, D.F. Hayes, P.K. McAllister, R.F. Morton, R.L. Schilsky, American Society of Clinical Oncology provisional clinical opinion: testing for KRAS gene mutations in patients with metastatic colorectal carcinoma to predict response to anti-epidermal growth factor receptor monoclonal antibody therapy, J. Clin. Oncol. 27 (12) (2009) 2091–2096.

[8] U. Malapelle, C. Carlomagno, C. de Luca, C. Bellevicine, G. Troncone, KRAS testing in metastatic colorectal carcinoma: challenges, controversies, breakthroughs and beyond, J. Clin. Pathol. 67 (1) (2014) 1–9.

[9] D. Krikelis, E. Skoura, V. Kotoula, P. Rondogianni, N. Pianou, A. Samartzis, I. Xanthakis, G. Fountzilas, I.E. Datseris, Lack of association between KRAS mutations and 18F-FDG PET/CT in Caucasian metastatic colorectal cancer patients, Anticancer Res. 34 (5) (2014) 2571–2579.

[10] P. Lovinfosse, B. Koopmansch, F. Lambert, S. Jodogne, G. Kustermans, M. Hatt, D. Visvikis, L. Seidel, M. Polus, A. Albert, P. Delvenne, R. Hustinx, (18)F-FDG PET/CT imaging in rectal cancer: relationship with the RAS mutational status, Br. J. Radiol. 89 (1063) (2016) 20160212.

[11] S.W. Chen, H.C. Chiang, W.T. Chen, T.C. Hsieh, K.Y. Yen, S.F. Chiang, C.H. Kao, Correlation between PET/CT parameters and KRAS expression in colorectal cancer, Clin. Nucl. Med. 39 (8) (2014) 685–689.

[12] K. Kawada, K. Toda, Y. Nakamoto, M. Iwamoto, E. Hatano, F. Chen, S. Hasegawa, K. Togashi, H. Date, S. Uemoto, Y. Sakai, Relationship between 18F-FDG PET/CT scans and KRAS mutations in metastatic colorectal Cancer, J. Nucl. Med. 56 (9) (2015) 1322–1327.

[13] A. Cho, K. Jo, S.H. Hwang, N. Lee, M. Jung, M. Yun, H.S. Hwang, Correlation between KRAS mutation and (18)F-FDG uptake in stage IV colorectal cancer, Abdom. Radiol. (NY) 42 (6) (2017) 1621–1626.

[14] M.G. Lubner, A.D. Smith, K. Sandrasegaran, D.V. Sahani, P.J. Pickhardt, CT Texture Analysis: Definitions, Applications, Biologic Correlates, and Challenges, Radiographics : a review publication of the Radiological Society of North America, Inc 37 (5) (2017) 1483–1503.

[15] C.E. Atreya, R. Yaeger, E. Chu, Systemic therapy for metastatic colorectal Cancer: from current standards to future molecular targeted approaches, american society of clinical oncology educational book, American Society of Clinical Oncology. Annual Meeting 37 (2017) 246–256.

[16] J. Beech, T. Germetaki, M. Judge, N. Paton, J. Collins, A. Garbutt, M. Braun, J. Fenwick, M.P. Saunders, Management and grading of EGFR inhibitor-induced cutaneous toxicity, Future Oncol. 14 (24) (2018) 2531–2541.

[17] V. Heinemann, L.F. von Weikersthal, T. Decker, A. Kiani, U. Vehling-Kaiser, S.E. Al-Batran, T. Heintges, C. Lerchenmuller, C. Kahl, G. Seipelt, F. Kullmann, M. Stauch, W. Scheithauer, J. Hielscher, M. Scholz, S. Muller, H. Link, N. Niederle, A. Rost, H.G. Hoffkes, M. Moehler, R.U. Lindig, D.P. Modest, L. Rossius, T. Kirchner, A. Jung, S. Stintzing, FOLFIRI plus cetuximab versus FOLFIRI plus bevacizumab as first-line treatment for patients with metastatic colorectal cancer (FIRE-3): a randomised, open-label, phase 3 trial, Lancet Oncol. 15 (10) (2014) 1065–1075.

[18] S.E. Baldus, K.L. Schaefer, R. Engers, D. Hartleb, N.H. Stoecklein, H.E. Gabbert, Prevalence and heterogeneity of KRAS, BRAF, and PIK3CA mutations in primary colorectal adenocarcinomas and their corresponding metastases, Clin. Cancer Res. 16 (3) (2010) 790–799.
[19] M. Iwamoto, K. Kawada, Y. Nakamoto, Y. Itatani, S. Inamoto, K. Toda, H. Kimura, T. Sasazuki, S. Shirasawa, H. Okuyama, M. Inoue, S. Hasegawa, K. Togashi, Y. Sakai, Regulation of 18F-FDG accumulation in colorectal cancer cells with mutated KRAS, Journal of nuclear medicine : official publication, Indian J. Nucl. Med. 55 (12) (2014) 2038–2044.
[20] J.H. Lee, J. Kang, S.H. Baik, K.Y. Lee, B.J. Lim, T.J. Jeon, Y.H. Ryu, S.K. Sohn, Relationship between 18F-Fluorodeoxyglucose uptake and V-Ki-Ras2 kirsten rat sarcoma viral oncogene homolog mutation in colorectal Cancer patients: variability depending on C-Reactive protein level, Medicine 95 (1) (2016) e2236.
[21] S.J. Kim, K. Pak, K. Kim, Diagnostic performance of F-18 FDG PET/CT for prediction of KRAS mutation in colorectal cancer patients: a systematic review and meta-analysis, Abdom. Radiol. (NY) 95 (1) (2016) e2236.
[22] X. Meng, W. Xia, P. Xie, R. Zhang, W. Li, M. Wang, F. Xiong, Y. Liu, X. Fan, Y. Xie, X. Wan, K. Zhu, H. Shan, L. Wang, X. Gao, Preoperative radiomic signature based on multiparametric magnetic resonance imaging for noninvasive evaluation of biological characteristics in rectal cancer, Eur. Radiol. 29 (6) (2019) 3200–3209.
[23] Y.R. Shin, K.A. Kim, S. Im, S.S. Hwang, K. Kim, Prediction of KRAS mutation in rectal Cancer Using MRI, Anticancer Res. 36 (9) (2016) 4799–4804.
[24] Y. Xu, Q. Xu, H. Sun, T. Liu, K. Shi, W. Wang, Could IVIM and ADC help in predicting the KRAS status in patients with rectal cancer? Eur. Radiol. 28 (7) (2018) 3059–3065.
[25] D.M. Yeo, S.N. Oh, M.H. Choi, S.H. Lee, M.A. Lee, S.E. Jung, Histogram Analysis of Perfusion Parameters from Dynamic Contrast-Enhanced MR Imaging with Tumor Characteristics and Therapeutic Response in Locally Advanced Rectal Cancer, Biomed Res. Int. 2018 (2018) 3724393.
[26] L. Yang, D. Dong, M. Fang, Y. Zhu, Y. Zang, Z. Liu, H. Zhang, J. Ying, X. Zhao, J. Tian, Can CT-based radiomics signature predict KRAS/NRAS/BRAF mutations in colorectal cancer? Eur. Radiol. 28 (5) (2018) 2058–2067.
[27] W. De Roock, H. Piessevaux, J. De Schutter, M. Janssens, G. De Hertogh, N. Personeni, B. Biesmans, J.L. Van Laethem, M. Peeters, Y. Humblet, E. Van Cutsem, S. Tejpar, KRAS wild-type state predicts survival and is associated to early radiological response in metastatic colorectal cancer treated with cetuximab, Annals of oncology: official journal of the European Society for Medical Oncology 19 (3) (2008) 508–515.
[28] M.G. Lubner, N. Stabo, S.J. Lubner, A.M. del Rio, C. Song, R.B. Halberg, P.J. Pickhardt, CT textural analysis of hepatic metastatic colorectal cancer: pre-treatment tumor heterogeneity correlates with pathology and clinical outcomes, Abdom. Imaging 40 (7) (2015) 2331–2337.
[29] F. Ng, R. Kozarski, B. Ganeshan, V. Goh, Assessment of tumor heterogeneity by CT texture analysis: can the largest cross-sectional area be used as an alternative to whole tumor analysis? Eur. J. Radiol. 82 (2) (2013) 342–348.